Infrared absorption of $C_6H_5SO_2$ detected with time-resolved Fourier-transform spectroscopy

Li-Kang Chu and Yuan-Pern Lee

Citation: The Journal of Chemical Physics **126**, 134311 (2007); doi: 10.1063/1.2713110
View online: http://dx.doi.org/10.1063/1.2713110
View Table of Contents: http://scitation.aip.org/content/aip/journal/jcp/126/13?ver=pdfcov
Published by the AIP Publishing

Infrared absorption of $C_6H_5SO_2$ detected with time-resolved Fourier-transform spectroscopy

Li-Kang Chu and Yuan-Pern Lee[a)]
Department of Applied Chemistry, National Chiao Tung University, Hsinchu 30010, Taiwan; Institute of Molecular Science, National Chiao Tung University, Hsinchu 30010, Taiwan; and Institute of Atomic and Molecular Sciences, Academia Sinica, Taipei 10617, Taiwan

(Received 7 December 2006; accepted 7 February 2007; published online 5 April 2007)

$C_6H_5SO_2$ radicals were produced upon irradiation of three flowing mixtures: $C_6H_5SO_2Cl$ in N_2, C_6H_5Cl and SO_2 in CO_2, and C_6H_5Br and SO_2 in CO_2, with a KrF excimer laser at 248 nm. A step-scan Fourier-transform spectrometer coupled with a multipass absorption cell was employed to record the time-resolved infrared (IR) absorption spectra of reaction intermediates. Two transient bands with origins at 1087.7 and 1278.2 cm^{-1} are assigned to the SO_2-symmetric and SO_2-antisymmetric stretching modes, respectively, of $C_6H_5SO_2$. Calculations with density-functional theory (B3LYP/aug-cc-pVTZ and B3P86/aug-cc-pVTZ) predict the geometry and vibrational wave numbers of $C_6H_5SO_2$ and C_6H_5OSO. The vibrational wave numbers and IR intensities of $C_6H_5SO_2$ agree satisfactorily with the observed new features. Rotational contours of IR spectra of $C_6H_5SO_2$ simulated based on predicted molecular parameters agree satisfactorily with experimental results for both bands. The SO_2-symmetric stretching band is dominated by *a*- and *c*-type rotational structures and the SO_2-antisymmetric stretching band is dominated by a *b*-type rotational structure. When $C_6H_5SO_2Cl$ was used as a precursor of $C_6H_5SO_2$, $C_6H_5SO_2Cl$ was slowly reproduced at the expense of $C_6H_5SO_2$, indicating that the reaction $Cl+C_6H_5SO_2$ takes place. When $C_6H_5Br/SO_2/CO_2$ was used as a precursor of $C_6H_5SO_2$, features at 1186 and 1396 cm^{-1} ascribable to $C_6H_5SO_2Br$ were observed at a later period due to secondary reaction of $C_6H_5SO_2$ with Br. Corresponding kinetics based on temporal profiles of observed IR absorption are discussed. © *2007 American Institute of Physics*. [DOI: 10.1063/1.2713110]

I. INTRODUCTION

The benzenesulfonyl radical ($C_6H_5SO_2$) is an important intermediate in organic syntheses.[1] Although investigation of the reaction between C_6H_5 and SO_2 is unreported, formation of $C_6H_5SO_2$ is expected to be rapid; hence $C_6H_5SO_2$ might also play an important role in the coupling of cycles involving SO_x and aromatic compounds in the atmosphere.

Previous investigations involving electron-paramagnetic-resonance (EPR) spectra of sulfonyl radicals produced in solutions containing arylsulphinic acid or sulphonyl halides indicated that these radicals have a σ-type structure with the unpaired electron localized on the SO_2 moiety. The half-filled orbital lies approximately on a plane containing the benzene ring.[2–5] Semiempirical calculations with intermediate neglect of differential overlap also support the σ character and in-plane radical structure of $C_6H_5SO_2$.[5] UV absorption of $C_6H_5SO_2$ in solution shows a broad band with an onset of ~500 nm and a maximum in the range of 315–335 nm, depending on the solvent.[6,7] Multiple-scattering $X\alpha$ calculations indicate that this band is associated with excitation of the electron from oxygen to the half-filled molecular orbital that is effectively localized on the SO_2 moiety.[6] Some kinetic studies of $C_6H_5SO_2$ in solution were conducted by probing its EPR spectrum[8] or the UV absorption band.[7] No spectral or kinetic information of $C_6H_5SO_2$ in the gaseous phase has been reported. Hence it is desirable to develop a detection technique to investigate the spectra and reaction kinetics of $C_6H_5SO_2$.

By coupling a step-scan Fourier-transform spectrometer (FTS) with a multipass absorption cell, we have demonstrated that we can record time-resolved infrared (IR) absorption spectra of gaseous reaction intermediates, such as ClCO,[9] ClSO,[10] and CH_3SO_2,[11] and species in vibrationally excited states (HCl^* and CH_4^*).[12,13] Here we report an application of time-resolved (FTS) to record IR absorption spectra of the intermediate $C_6H_5SO_2$ and its secondary reaction products $C_6H_5SO_2Cl$ and $C_6H_5SO_2Br$.

II. EXPERIMENTS

In a commercial Fourier-transform spectrometer (Thermo Nicolet, Nexus 870), the moving mirror is stepped, and holds its position at each step within ±0.2 nm.[14] White cell with a base path length of 20 cm and an effective path length of 6.4 m was placed in the sample compartment of the spectrometer.[10,11] The volume of the cell is ~2.0 L. The housing of the white cell accommodates two rectangular (3×12 cm^2) quartz windows to pass photolysis beams that propagate perpendicular to multipassing IR beams. The photolysis laser beam passes these quartz windows and is multiply reflected between a pair of external laser mirrors. A KrF excimer laser (Lambda Physik, LPX120i, 11 Hz) emitting at

a)Author to whom correspondence should be addressed. Fax: 886-3-5713491; Electronic mail: yplee@mail.nctu.edu.tw

248 nm is slightly focused and employed for photodissociation of $C_6H_5SO_2Cl$ in N_2. Its typical output energy is ~85 mJ pulse^{-1}, with a beam dimension of $\sim 4\times 11$ mm^2. Another KrF excimer laser (Gam Laser, EX100H/60, 10 Hz) is slightly expanded and employed for photolysis of flowing mixtures of $C_6H_5Cl/SO_2/CO_2$ and $C_6H_5Br/SO_2/CO_2$. Its typical output is ~50 mJ pulse^{-1}, with a beam dimension of $\sim 15\times 20$ mm^2.

Techniques to derive time-resolved difference absorption spectra from interferograms recorded with ac- and dc-coupled signals are well established.[9,15] After preamplification, the ac-coupled signal from the MgCdTe detector (20 MHz) was further amplified (Stanford Research Systems, Model SR560, using a bandwidth of 300 Hz–1 MHz) 20 times before sending to a 14 bit digitizer (Gage Applied Technology, CompuScope 14100, 10^8 samples s^{-1}). The dc-coupled signal from the MCT detector was sent directly to the internal 16 bit digitizer (2×10^5 samples s^{-1}) of the spectrometer. Typically, 800 data points were acquired at 0.2 μs integrated intervals (20 dwells at 10 ns gate width) for a period of 160 μs after photolysis. The signal is typically averaged over 50 laser shots at each scan step. With appropriate optical filters to define a small spectral region, we performed undersampling to decrease the number of points in the interferogram, hence the duration of data acquisition. For spectra in the range of 850–1580 cm^{-1} at a resolution of 2.0 cm^{-1}, 960 scan steps were completed within ~80 min. To improve further the signal to noise ratio, we recorded and averaged seven sets of data under similar experimental conditions upon photolysis of $C_6H_5SO_2Cl$. For photolysis of flowing mixtures of $C_6H_5Br/SO_2/CO_2$ and $C_6H_5Cl/SO_2/CO_2$, no average of similar spectra was performed.

We used flowing mixtures of three types: $C_6H_5SO_2Cl$ in N_2, C_6H_5Cl and SO_2 in CO_2, and C_6H_5Br and SO_2 in CO_2. Experimental conditions for photolysis of $C_6H_5SO_2Cl$ are as follows: flow rates $F_{C_6H_5SO_2Cl}=0.1$ cm^3 s^{-1} STP and $F_{N_2}=23.6$ cm^3 s^{-1} STP (STP denotes standard temperature 273.15 K and pressure 1 atm), with a total pressure of ~72.0 Torr. In separate experiments, C_6H_5Cl and C_6H_5Br were photolyzed to yield C_6H_5, followed by reaction with SO_2. The efficiencies of photolysis of C_6H_5Cl and C_6H_5Br are estimated to be ~0.2% and 0.8%, respectively, based on their absorption cross sections at 248 nm ($\sim 1.0\times 10^{-19}$ and 3.8×10^{-19} cm^2 molecule^{-1} for C_6H_5Cl and C_6H_5Br, respectively),[16,17] the effective path length is ~34 cm, and the laser fluence is $\sim 2.0\times 10^{16}$ photons cm^{-2}. We found that vibrationally excited SO_2 was produced upon irradiation, and CO_2 was employed as an efficient quencher to minimize interference due to excited SO_2. For experiments with $C_6H_5Cl/SO_2/CO_2$, the flow rates were $F_{C_6H_5Cl}=0.18$ cm^3 s^{-1} STP, $F_{SO_2}=1.13$ cm^3 s^{-1} STP, and $F_{CO_2}=13.7$ cm^3 s^{-1} STP, and the total pressure was ~25.1 Torr. For experiments with $C_6H_5Br/SO_2/CO_2$, the flow rates were $F_{C_6H_5Br}=0.09$ cm^3 s^{-1} STP, $F_{SO_2}=1.1$ cm^3 s^{-1} STP, and $F_{CO_2}=13.8$ STP cm^3 s^{-1}, and the total pressure was ~24.1 Torr.

$C_6H_5SO_2Cl$ (>99%, Alfa Aesar), C_6H_5Cl, C_6H_5Br (both >99%, Acros), SO_2 (>99%, anhydrous, Matheson), and N_2 (99.999%, AGA Specialty Gases) were used without further purification. CO_2 (99.99%, AGA Specialty Gases) was purified on passage through a trap at 218 K. In experiments with $C_6H_5SO_2Cl$, the temperature of the sample tube and the white cell was maintained at 353 K to increase the vapor pressure of $C_6H_5SO_2Cl$ and to avoid condensation.

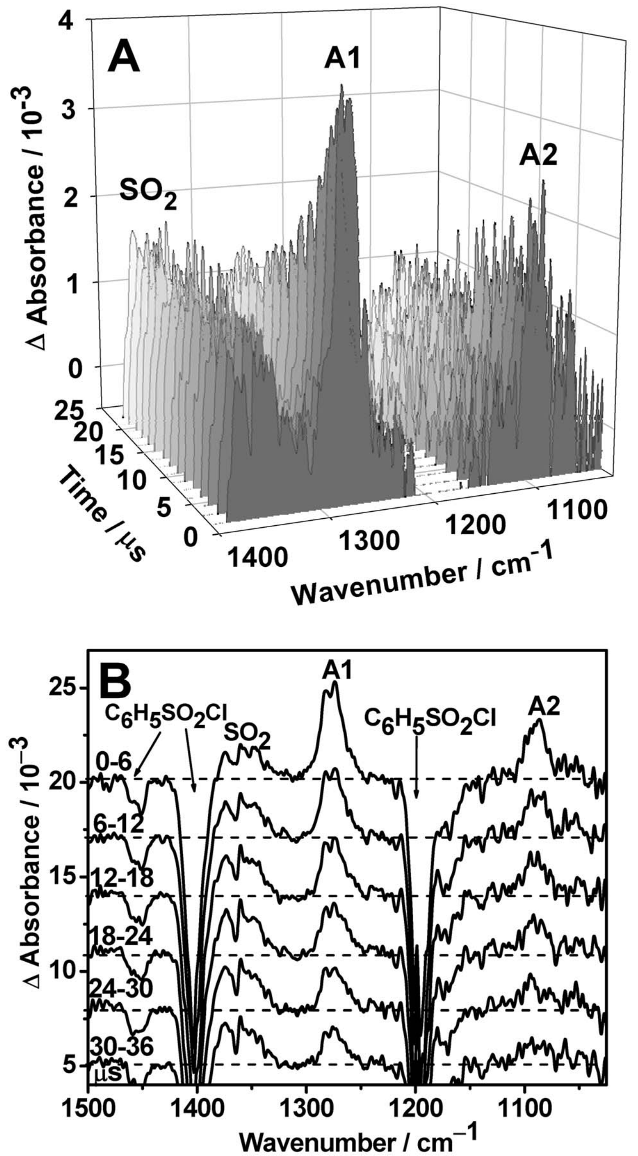

FIG. 1. (A) Three-dimensional plot of time-resolved spectra upon laser photolysis (248 nm, 11 Hz, 190 mJ cm^{-2}) of a flowing mixture of $C_6H_5SO_2Cl/N_2$ (1/240) at 72 Torr and 353 K. The path length is 6.4 m and the resolution is 2.0 cm^{-1}. (B) Spectra averaged at 6 μs intervals. The upward features correspond to formation of SO_2 and $C_6H_5SO_2$ (indicated as A1 and A2), whereas the downward features are due to destruction of the precursor of $C_6H_5SO_2Cl$.

III. THEORETICAL CALCULATIONS

The equilibrium geometry, vibrational wave numbers, and IR intensities of $C_6H_5SO_2$ and C_6H_5OSO were calculated with B3LYP and B3P86 density-functional theory using the GAUSSIAN 03 program.[18] The B3LYP method uses Becke's three-parameter hybrid exchange functional with a correlation functional of Lee, Yang, and Parr.[19,20] The B3P86 method uses Becke's three-parameter hybrid exchange func-

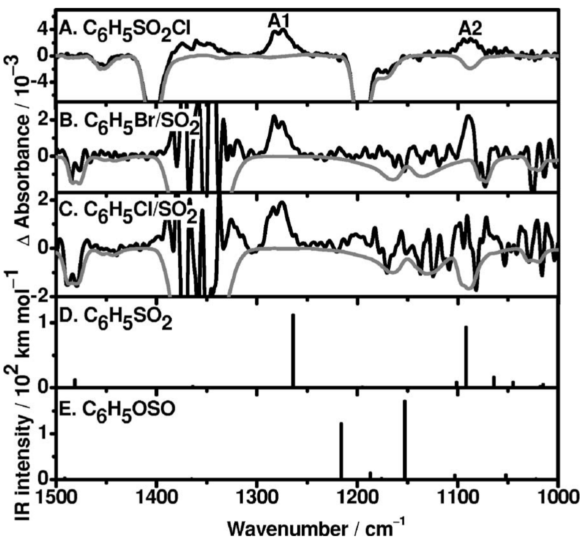

FIG. 2. Transient absorption spectra recorded upon 248 nm photolysis of three flowing mixtures: (A) $C_6H_5SO_2Cl/N_2$ (1/240) at 72 Torr and 353 K (the resolution is 2 cm^{-1} and the averaging period is 0–7 μs); (B) $C_6H_5Br/SO_2/CO_2$ (1/12/150) at 24.1 Torr and 298 K (the resolution is 3 cm^{-1} and the averaging period is 5–57 μs); and (C) $C_6H_5Cl/SO_2/CO_2$ (1/6.3/76) at 25.1 Torr and 298 K (the resolution is 3 cm^{-1} and the averaging period is 5–57 μs). (D) Stick spectra of $C_6H_5SO_2$ and (E) C_6H_5OSO, both are based on unscaled harmonic vibrational wave numbers and IR intensities predicted with the B3P86/aug-cc-pVTZ method.

tional with Perdew's gradient-corrected correlation functional.[21] Dunning's correlation-consistent polarized-valence triple-zeta basis sets, augmented with *s*, *p*, *d*, and *f* functions (aug-cc-pVTZ),[22,23] and standard 6-311++G** basis sets were applied in these calculations. Analytic first derivatives were utilized in geometry optimization, and harmonic vibrational wave numbers were calculated analytically at each stationary point. Comparison of rotational parameters of the ground and vibrationally excited ($v_i=1$) states were performed with the B3P86/6-311+G** method. Molecular parameters of $C_6H_5SO_2X$ (X=F, Cl, and Br) were predicted with B3P86/6-311G*.

IV. RESULTS AND DISCUSSION

As a test, conventional FTIR measurements were performed with a static cell containing 0.14 Torr of $C_6H_5SO_2Cl$. The absorption of $C_6H_5SO_2Cl$ is characterized by intense bands near 1404, 1455, and 3078 cm^{-1}.[24] After laser irradiation at 248 nm (10 Hz) for 120 s, absorption bands of SO_2 (1151, 1362, and 2499 cm^{-1}), HCl (2886 cm^{-1}), and C_6H_5Cl (3084 cm^{-1}) as end products were observed. No absorption band detected in the static-cell experiment is ascribable to $C_6H_5SO_2$.

A. Photolysis of $C_6H_5SO_2Cl$ in N_2 and C_6H_5X (X=Cl or Br)/SO_2 in CO_2

Our previous experience indicated that upon irradiation a fraction of the precursor became highly internally excited and yielded new upward-pointing features on each side of the downward parent band in the difference absorption spectrum. In this difference spectrum, features pointing upward indicate production, whereas those pointing downward indicate destruction. In many cases these two side lobs interfere with nearby absorption bands of photodissociation products and hamper their detection. Hence we added excessive quenchers such as N_2 or CO_2 to thermalize the species in the system.

A representative three-dimensional (3D) plot of temporally and spectrally resolved spectra at 1.5 μs intervals upon laser irradiation of a flowing mixture of ~72 Torr of $C_6H_5SO_2Cl/N_2$ (≅1/240) at 248 nm is shown in Fig. 1(A) (resolution 2 cm^{-1}). The spectral region 1150–1210 cm^{-1} is not plotted because of the intense downward band of parent molecules $C_6H_5SO_2Cl$. The spectra integrated over 6 μs intervals are shown in Fig. 1(B). The downward features of the parent, at 1197, 1404, and 1455 cm^{-1}, are due to loss upon irradiation. The SO_2 absorption near 1362 cm^{-1} was observed to increase within ~3 μs and remained nearly constant afterwards. Two new features with maxima near 1278 and 1088 cm^{-1} (marked as A1 and A2, respectively) appeared immediately after irradiation, and decayed with time. These features have vibrational wave numbers similar to, but smaller than, those of the SO_2-antisymmetric and SO_2-symmetric stretching modes of $C_6H_5SO_2Cl$ at 1404 and 1197 cm^{-1} and of SO_2 at 1362 and 1151 cm^{-1}, respectively.[25]

The spectrum integrated over 5–57 μs upon photolysis of a flowing mixture of $C_6H_5Br/SO_2/CO_2$ (1/12/150, total pressure ~24.1 Torr) at 248 nm is shown in trace (B) of Fig. 2. The absorption spectrum of the parents (C_6H_5Br and SO_2)

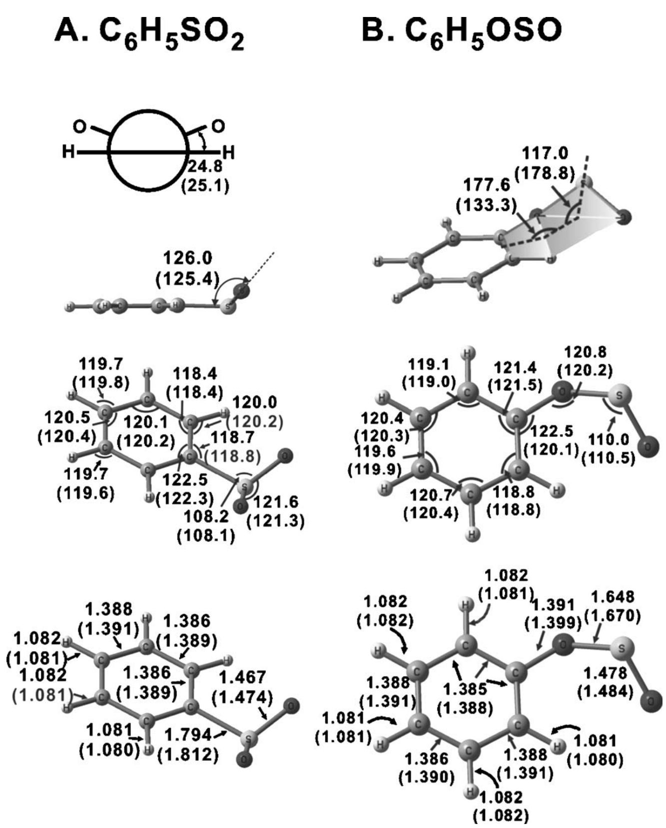

FIG. 3. Molecular structures predicted with B3P86/aug-cc-pVTZ and B3LYP/aug-cc-pVTZ methods for $C_6H_5SO_2$ (A) and C_6H_5OSO (B). The bond lengths are in angstrom and bond angles are in degree. Results from B3LYP are listed in parentheses.

TABLE I. Comparison of energies and rotational parameters of $C_6H_5SO_2$ and C_6H_5OSO derived from B3LYP and B3P86 calculations.

		$C_6H_5SO_2$		C_6H_5OSO	
		B3LYP	B3P86	B3LYP	B3P86
$E+780$/hartree[a]		−0.300 697	−1.617 095	−0.321 605	−1.634 231
Equilibrium[a]	A/cm^{-1}	0.115 12	0.115 79	0.118 82	0.133 07
	B/cm^{-1}	0.033 29	0.033 69	0.029 29	0.028 34
	C/cm^{-1}	0.026 19	0.026 45	0.025 41	0.024 03
$v=0$[b]	A/cm^{-1}		0.113 91		
	B/cm^{-1}		0.033 37		
	C/cm^{-1}		0.026 18		
$v=1$[b] SO_2-sym. str.	A/cm^{-1}		0.113 74		
	B/cm^{-1}		0.033 36		
	C/cm^{-1}		0.026 17		
$v=1$[b] SO_2-antisym. str.	A/cm^{-1}		0.113 68		
	B/cm^{-1}		0.033 36		
	C/cm^{-1}		0.026 17		

[a]Using basis sets aug-cc-pVTZ.
[b]Using basis sets $6-311+G^{**}$.

is shown as downward gray lines for comparison. In this experiment, although both features near 1278 (A1) and 1088 (A2) cm^{-1} are observed, the low-energy side of the feature near 1088 cm^{-1} is interfered with downward parent absorption band. The spectrum recorded over 0–7 μs after irradiation of $C_6H_5SO_2Cl/N_2$ is shown in trace (A) of Fig. 2 for comparison.

The spectrum integrated over 5–57 μs upon photolysis of a flowing mixture of $C_6H_5Cl/SO_2/CO_2$ (1/6.3/76, total pressure ~25.1 Torr) at 248 nm is shown in trace (C) of Fig. 2. The absorption spectrum of the parents (C_6H_5Cl and SO_2) is shown as downward gray lines for comparison. Because regions saturated with parent absorption overlap with that of the A2 band, only the A1 band at 1278 cm^{-1} was observed.

Among all three experiments, the quality of the spectrum recorded upon photolysis of $C_6H_5SO_2Cl$ is the best because absorption bands of the parent are less intense and well separated from those of the product, hence minimizing the interference. This spectrum is used for comparison with spectral simulations to be discussed later.

B. Quantum-chemical calculations on $C_6H_5SO_2$ and C_6H_5OSO

Reaction of C_6H_5 and SO_2 might form $C_6H_5SO_2$ and C_6H_5OSO. Geometries of $C_6H_5SO_2$ and C_6H_5OSO calculated with B3P86/aug-cc-pVTZ are shown in Figs. 3(A) and 3(B), respectively. Those calculated with B3LYP/aug-cc-pVTZ are listed parenthetically. For $C_6H_5SO_2$, the C–S bond length of 1.794 Å predicted in this work is slightly smaller than the experimental value of 1.818 Å for CH_3SH.[26] The predicted S═O bond length of 1.467 Å is slightly greater than the experimental value of 1.432 Å for SO_2 (Ref. 27) and the calculated value of 1.450 Å for $ClSO_2$.[28] For C_6H_5OSO, the optimized geometries derived with B3P86 and B3LYP/aug-cc-pVTZ methods are distinctly different, as indicated in Fig. 3(B). The two O atoms of C_6H_5OSO predicted with B3P86 are almost coplanar with the benzene ring, whereas the OSO and C_6H_5 planes were predicted with B3LYP to have a dihedral angle of ~133°. Except for this, the deviations in bond lengths and bond angles predicted with these two methods are small. For C_6H_5OSO the S═O bond length of 1.478 Å predicted with the B3P86 method is similar to that of SO_2, and the S–O bond length of 1.648 Å is similar to the predicted value of 1.638 Å for CH_3OSO.[11]

Rotational parameters for equilibrium geometries of $C_6H_5SO_2$ and C_6H_5OSO predicted with B3P86 and B3LYP methods using the aug-cc-pVTZ basis sets are listed in Table I for comparison. The difference in geometries of $C_6H_5SO_2$ predicted with B3LYP and B3P86 results in variations of rotational parameters less than 1.2%, whereas that of C_6H_5OSO is ~12% due to greater deviations in geometry. Rotational parameters of $C_6H_5SO_2$ vibrationally excited in the SO_2-symmetric stretching and SO_2-antisymmetric stretching modes, calculated with the B3P86/6-311++G^{**} method, are also listed in Table I. They are useful for simulation of observed spectra.

Unscaled harmonic vibrational wave numbers and IR intensities of $C_6H_5SO_2$ and C_6H_5OSO predicted with B3LYP and B3P86/aug-cc-pVTZ methods are compared in Table II. The two most intense bands of $C_6H_5SO_2$ predicted with B3P86 (B3LYP) methods are at 1264 (1227) and 1092 (1072) cm^{-1}, corresponding to the SO_2-antiymmetric and SO_2-symmetric stretching modes, respectively. The latter mode is mixed with some C–S stretching motion. Two medium intense bands predicted near 766 and 518 cm^{-1} are outside the range of our detection. Previous predictions of vibrational wave numbers for the SO_2-antisymmetric and SO_2-symmetric stretching modes of CH_3SO_2 using the aug-cc-pVTZ basis sets deviate within 4.4% (for B3LYP) and 1.4% (for B3P86) from experiments.[11] The four most intense bands of C_6H_5OSO predicted with B3P86 (B3LYP) methods are at 864 (841), 1153 (1137), 1216 (1201), and

TABLE II. Comparison of harmonic vibrational wave numbers (cm^{-1}, unscaled) and IR intensities ($km\ mol^{-1}$, listed parenthetically) of $C_6H_5SO_2$ and C_6H_5OSO derived from B3LYP and B3P86/aug-cc-pVTZ calculations.

$C_6H_5SO_2$		C_6H_5OSO	
B3LYP	B3P86	B3LYP	B3P86
54 (1)	56 (1)	30 (1)	23 (1)
142 (2)	142 (2)	62 (5)	57 (6)
177 (1)	176 (1)	106 (2)	136 (1)
289 (3)	295 (3)	242 (0)	243 (1)
362 (0)	366 (0)	344 (2)	296 (1)
392 (16)	393 (13)	426 (0)	420 (0)
410 (0)	406 (0)	450 (10)	457 (16)
478 (41)	483 (41)	475 (21)	497 (9)
517 (32)	518 (33)	572 (6)	548 (7)
625 (0)	620 (0)	630 (1)	624 (3)
689 (3)	690 (19)	684 (63)	698 (24)
697 (22)	696 (5)	708 (34)	725 (51)
768 (51)	766 (53)	790 (47)	776 (62)
862 (0)	861 (0)	841 (142)	845 (3)
956 (2)	953 (2)	849 (11)	864 (216)
1004 (0)	1000 (0)	937 (7)	925 (6)
1015 (14)	1015 (5)	992 (0)	986 (0)
1024 (1)	1018 (2)	1013 (0)	1003 (0)
1032 (25)	1045 (8)	1024 (0)	1022 (1)
1049 (21)	1064 (16)	1046 (9)	1052 (10)
1072 (57)	1092 (93)	1097 (8)	1103 (9)
1100 (7)	1101 (8)	1137 (123)	1153 (171)
1185 (0)	1181 (0)	1176 (55)	1176 (2)
1199 (2)	1195 (1)	1182 (5)	1187 (14)
1227 (106)	1264 (112)	1201 (53)	1216 (122)
1330 (1)	1333 (0)	1323 (1)	1336 (0)
1348 (3)	1364 (2)	1350 (0)	1365 (1)
1480 (11)	1481 (12)	1488 (3)	1491 (3)
1506 (6)	1505 (6)	1520 (59)	1524 (90)
1613 (1)	1629 (1)	1629 (24)	1646 (39)
1621 (0)	1638 (0)	1632 (6)	1651 (20)
3174 (0)	3188 (0)	3169 (0)	3185 (0)
3185 (8)	3199 (7)	3179 (8)	3194 (7)
3194 (5)	3208 (3)	3190 (15)	3206 (11)
3207 (0)	3218 (0)	3197 (5)	3214 (3)
3208 (8)	3219 (9)	3211 (0)	3218 (1)

1524 (1520) cm^{-1}, corresponding to the mixed antisymmetric O–S and C–O stretching, S=O stretching, C–O stretching, and C_6H_5 in-plane deformation modes, respectively. Two medium intense bands predicted near 776 and 725 cm^{-1} are outside the range of our detection.

The three rotational axes *a*, *b*, and *c* of $C_6H_5SO_2$ are indicated as arrows with dashed lines in Fig. 4. The *c* axis is nearly perpendicular to the plane containing the benzene ring. Predicted displacement vectors (thin arrows) and the associated dipole derivatives (thick arrows) for the SO_2-antisymmetric and SO_2-symmetric stretching modes of $C_6H_5SO_2$ are also shown in Figs. 4(A) and 4(B), respectively.

C. Assignment of $C_6H_5SO_2$

The major product on photolysis of $C_6H_5SO_2Cl$ is expected to be $C_6H_5SO_2+Cl$, as was observed in EPR

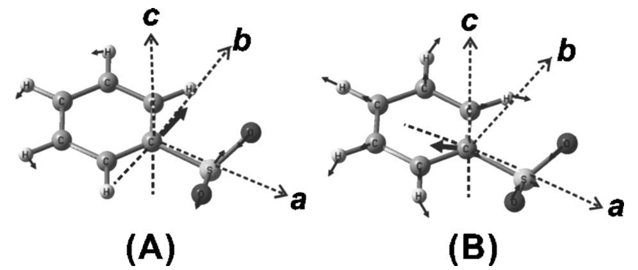

FIG. 4. Displacement vectors (thin arrows) and direction of dipole derivatives (thick arrow) predicted with the B3P86/aug-cc-pVTZ method for SO_2-antisymmetric stretching (A) and SO_2-symmetric stretching modes (B) of $C_6H_5SO_2$. Rotational axes *a*, *b*, and *c* are also shown with dash axis lines.

experiments.[8] EPR experiments using selective spin traps indicate, however, that the other channel, $C_6H_5+SO_2Cl$, also occurs when $C_6H_5SO_2Cl$ is irradiated with a 500 W Hg lamp.[29] The major products for photolysis of C_6H_5X (X=Cl or Br) are C_6H_5 and X.[30,31] Further reaction of C_6H_5 with SO_2 might form $C_6H_5SO_2$ or C_6H_5OSO. Except for the experiment of $C_6H_5Cl/SO_2/CO_2$ in which parent absorption interfered strongly with the A2 band, bands A1 (1278 cm^{-1}) and A2 (1088 cm^{-1}) were observed in all experiments, indicating that they are due to a common product, likely $C_6H_5SO_2$. These new features differ from the absorption band of SO at 1137.9 cm^{-1} (Ref. 32). Considering that these two new bands have wave numbers similar to, but slightly smaller than, those of SO_2 at 1361.8 and 1151.4 cm^{-1},[25] we expect that the carrier of these bands contains a SO_2 moiety.

IR absorption spectra of $C_6H_5SO_2$ and C_6H_5OSO in the 1000–1500 cm^{-1} region predicted with B3P86/aug-cc-pVTZ are shown as stick diagrams in traces (D) and (E) of Fig. 2, respectively. Unscaled harmonic vibrational wave numbers are used and predicted intensities are represented by the height of the sticks. Two most intense bands predicted at 1264 and 1092 cm^{-1} for $C_6H_5SO_2$ fit satisfactorily with two observed new features, with errors of −1.1% and 0.4%, respectively. Typical errors for DFT calculations at this level are about 2%–3%. The separation of these two observed features (190 cm^{-1}) is also consistent with the calculated separation of 172 cm^{-1} for SO_2-symmetric and SO_2-antisymmetric stretching modes. These agreements further support the assignments of these bands to $C_6H_5SO_2$. The two most intense bands predicted for C_6H_5OSO in this spectral region are 1216 and 1153 cm^{-1}, deviating from experimental observations by −4.9% and 6.0%, respectively.

As derivation of rotational parameters from observed spectra is unlikely to be practicable with the present spectral resolution, we simulate the band contour using the molecular parameters predicted with B3P86/6-311++G** to compare with the observed spectra. The direction of the dipole derivative for the SO_2-antisymmetric stretching mode of $C_6H_5SO_2$ shown in Fig. 4(A) indicates that the associated rovibrational band is *b* type, whereas that for the SO_2-symmetric stretching mode [Fig. 4(B)] is mainly *a* type, with a small contribution of *c* type. The projections of the dipole derivatives for the SO_2-antisymmetric stretching and SO_2-symmetric stretching modes onto the *a*, *b*, and *c* axes are 0.0: 1.0: 0.0 and 0.8: 0.0: 0.2, respectively.

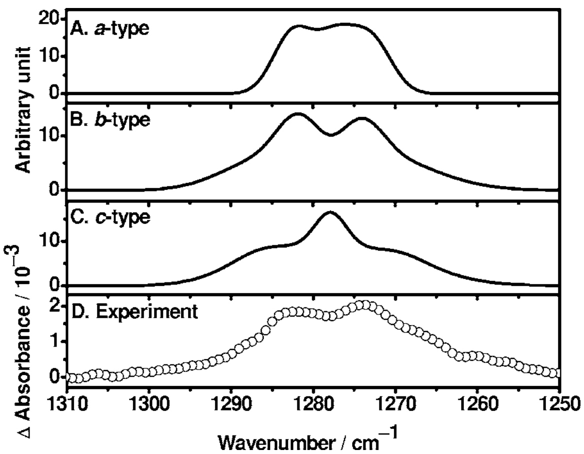

FIG. 5. Comparison of simulated and observed spectra of the SO_2-antisymmetric stretching mode of $C_6H_5SO_2$. The fitted parameters are $T=350$ K, $J_{max}=120$, $\nu_0=1278.2\ cm^{-1}$, $A''=0.113\,91\ cm^{-1}$, $B''=0.033\,37\ cm^{-1}$, $C''=0.026\,18\ cm^{-1}$, $A'=0.113\,68\ cm^{-1}$, $B'=0.033\,36\ cm^{-1}$, and $C'=0.026\,17\ cm^{-1}$. (A) *a*-type component, (B) *b*-type component, (C) *c*-type component, and (D) spectrum recorded at a resolution of 2 cm^{-1} and integrated for 0–6 μs after 248 nm laser irradiation of a flowing mixture of $C_6H_5SO_2Cl/N_2$ (1/240) at 353 K and 72 Torr.

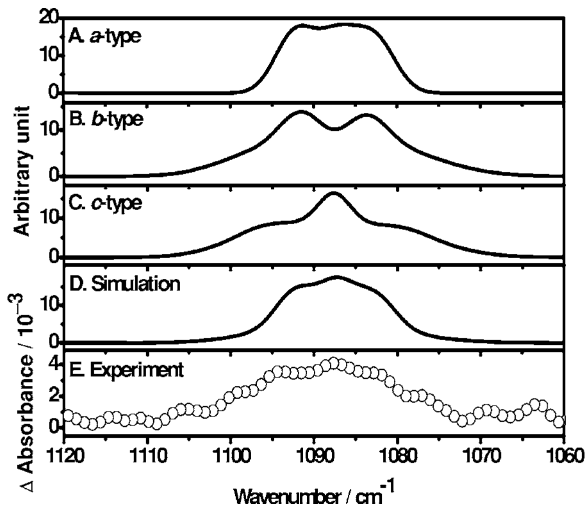

FIG. 6. Comparison of simulated and observed spectra of the SO_2-symmetric stretching mode of $C_6H_5SO_2$. The fitted parameters are $T=350$ K, $J_{max}=120$, $\nu_0=1087.7\ cm^{-1}$, $A''=0.113\,91\ cm^{-1}$, $B''=0.033\,37\ cm^{-1}$, $C''=0.026\,18\ cm^{-1}$, $A'=0.113\,74\ cm^{-1}$, $B'=0.033\,36\ cm^{-1}$, and $C'=0.026\,17\ cm^{-1}$. (A) *a*-type component, (B) *b*-type component, (C) *c*-type component, (D) simulated spectrum using a combination of *a* and *c* types with a ratio of 0.8: 0.2, and (E) spectrum recorded at a resolution of 2 cm^{-1} and integrated for 0–6 μs after 248 nm laser irradiation of a flowing mixture of $C_6H_5SO_2Cl/N_2$ (1/240) at 353 K and 72 Torr.

The spectrum of the SO_2-antisymmetric stretching band was simulated with the SPECVIEW program[33] using rotational parameters *A*, *B*, and *C* of both upper and lower states derived from B3P86/6-311++G** (Table I), with $J_{max}=120$, $T=350$ K, and a Doppler line shape with full width at half maximum (FWHM)=2.0 cm^{-1}. Simulated *a*-, *b*-, and *c*-type spectra are shown in traces (A)-(C) of Fig. 5, respectively. The experimental observation shown in trace (D) fits satisfactorily with the *b*-type band. This agreement in rotational contour further supports our assignment of this band to the SO_2-antisymmetric stretching mode of $C_6H_5SO_2$.

The spectrum of the SO_2-symmetric stretching band was also simulated using rotational parameters *A*, *B*, and *C* of both upper and lower states derived from quantum-chemical calculations (Table I), with $J_{max}=120$, $T=350$ K, and a Doppler line shape with FWHM=2.0 cm^{-1}. Simulated *a*-, *b*-, and *c*-type spectra are shown in traces (A)-(C) of Fig. 6, respectively. A simulated spectrum of $C_6H_5SO_2$ using a ratio of 0.8: 0.2 for *a*-type and *c*-type components is shown in trace (D). Although the signal to noise ratio is worse than that of the SO_2-antisymmetric stretching mode, our experimental observation shown in trace (E) fits satisfactorily with the simulation in trace (D).

D. Assignment of $C_6H_5SO_2Br$

The temporally resolved difference spectra of a 248 nm irradiated flowing mixture of $C_6H_5Br/SO_2/CO_2$ (1/4.4/118) at pressure 30.9 Torr, recorded at 50 μs intervals, are shown in Fig. 7(A) for the 1500–1000 cm^{-1} region. The features A1 and A2 have been assigned as the SO_2-antisymmetric and symmetric stretching modes of $C_6H_5SO_2$ in the previous section. As indicated in Fig. 7(A), new bands B1 and B2 appeared following the decay of $C_6H_5SO_2$. The contour of the B1 band at the low-energy side is interfered by the absorption of SO_2. Because C_6H_5 and Br are the main products upon irradiation of the flowing mixture $C_6H_5Br/SO_2/CO_2$, $C_6H_5SO_2Br$ and $(C_6H_5)_2SO_2$ are the most likely products in the secondary reactions of $C_6H_5SO_2$ with Br and C_6H_5, respectively.

The vibrational wave numbers of $(C_6H_5)_2SO_2$ in the 1100–1500 cm^{-1} region showed four intense bands near 1105, 1155, 1311, and 1450 cm^{-1},[24] which are distinctly different from our observed bands near 1396 and 1186 cm^{-1}. Infrared spectrum of $C_6H_5SO_2Br$ is unreported. The infrared absorption spectrum of $C_6H_5SO_2Br$ predicted with B3P86/6-311G* is shown as a stick diagram in Fig. 7(B).

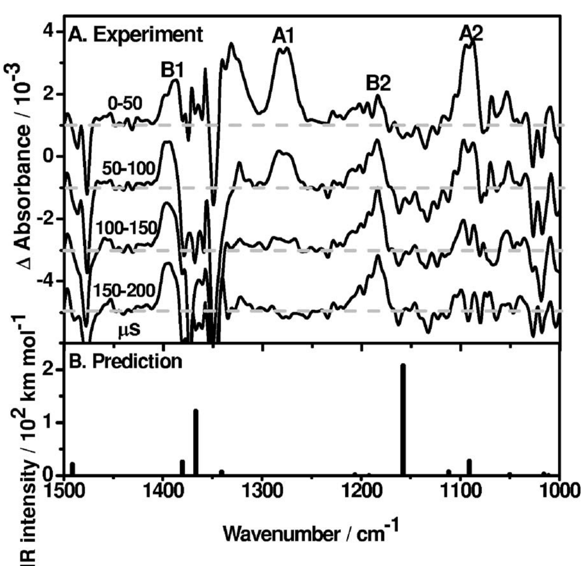

FIG. 7. (A) Temporally resolved spectra averaged at 50 μs intervals upon photolysis (248 nm, 10 Hz, 17 mJ cm^{-2}) of a flowing mixture of $C_6H_5Br/SO_2/CO_2$ (1/4.4/118) at 30.9 Torr. A1 and A2 bands are attributed to $C_6H_5SO_2$. B1 and B2 bands are assigned to $C_6H_5SO_2Br$. (B) Stick spectrum of $C_6H_5SO_2Br$ based on unscaled harmonic vibrational wave numbers and IR intensities predicted with the B3P86/6-311G* method.

TABLE III. Comparison of SO_2-antisymmetric and SO_2-symmetric stretching wave numbers (cm^{-1}) of $C_6H_5SO_2X$ (X=F, Cl, and Br) derived from B3P86/6−311G* calculations and from experiments.

	Calculations		Experiments		
	SO_2-antisym. str.	SO_2-sym. str.	SO_2-antisym. str.	SO_2-sym. str.	Reference
$C_6H_5SO_2F$	1416	1198	1434 (1.013)[a]	1224 (1.022)[a]	24
$C_6H_5SO_2Cl$	1388	1169	1399 (1.008)	1192 (1.020)	24
$C_6H_5SO_2Br$	1366	1156	1396 (1.022)	1186 (1.026)	This work

[a]Ratios of experimental to calculated vibrational wave numbers are listed in parentheses.

Unscaled harmonic vibrational wave numbers are used and the height of the stick represents the IR intensity in km mol^{-1}. Observed features at 1396 and 1186 cm^{-1} in Fig. 7(A) agree with predicted wave numbers of $C_6H_5SO_2Br$ satisfactorily. Vibrational wave numbers of SO_2-symmetric and SO_2-antisymmetric stretching modes of $C_6H_5SO_2F$ and $C_6H_5SO_2Cl$ have been reported.[24] Table III compares experimental and calculated (B3P86/6-311G*) wave numbers of these two vibrational modes of $C_6H_5SO_2X$ (X═F, Cl, and Br). The ratio of experimental to the calculated vibrational wave numbers of both the SO_2-antisymmetric and SO_2-symmetric stretching modes of $C_6H_5SO_2F$ and $C_6H_5SO_2Cl$ are in the range of 1.008–1.022. Corresponding ratios of 1.022 and 1.026 for the assignment of observed features at 1396 and 1186 cm^{-1} to $C_6H_5SO_2Br$ agree satisfactorily with those of $C_6H_5SO_2F$ and $C_6H_5SO_2Cl$. Hence, we assign the bands near 1396 and 1186 cm^{-1} to be the SO_2-antisymmetric and SO_2-symmetric stretching modes of $C_6H_5SO_2Br$, respectively.

E. Further reaction of $C_6H_5SO_2$

1. Photolysis of $C_6H_5SO_2Cl$ *in* N_2

As can be seen in the 3D plot of Fig. 1(A), intensities of these two new features (A1 and A2) near 1278 and 1088 cm^{-1} decay with time. Integrated spectra in Fig. 1(B) show more clearly the temporal behavior of these features. Not as obviously shown as those two features, absorption intensity of $C_6H_5SO_2Cl$ gradually recovered with reaction time after the initial depletion, as indicated in the downward features in the first few time slices of Fig. 1(B). Temporal profiles of bands corresponding to $C_6H_5SO_2$ (integrated over 1255–1295 cm^{-1}), SO_2 (1330–1380 cm^{-1}), and $C_6H_5SO_2Cl$ (1390–1420 cm^{-1}) are shown in Fig. 8.

A simple mechanism is proposed for photolysis of $C_6H_5SO_2Cl$,

$$C_6H_5SO_2Cl + h\nu \rightarrow C_6H_5SO_2 + Cl, \quad \Delta H = 300 \text{ kJ mol}^{-1}, \tag{1a}$$

$$C_6H_5SO_2Cl + h\nu \rightarrow C_6H_5 + ClSO_2, \quad \Delta H = 453 \text{ kJ mol}^{-1}, \tag{1b}$$

$$C_6H_5SO_2Cl + h\nu \rightarrow C_6H_5 + SO_2 + Cl, \quad \Delta H = 497 \text{ kJ mol}^{-1}, \tag{1c}$$

$$C_6H_5SO_2 + Cl \rightarrow C_6H_5SO_2Cl, \quad \Delta H = -300 \text{ kJ mol}^{-1}, \tag{2}$$

in which reaction (2) represents the recombination of Cl and $C_6H_5SO_2$. At 298 K, the enthalpy of formation of $C_6H_5SO_2Cl$, $C_6H_5SO_2$, C_6H_5, SO_2, Cl, and $ClSO_2$ are −334,[34] −155,[35] 339,[36] −297,[37] 121,[37] and −220 kJ mol^{-1},[28] respectively. The photon energy of 482 kJ mol^{-1} at 248 nm is greater than the enthalpy changes of reactions (1a) and (1b), but slightly smaller than that of reaction (1c).

The reaction of $C_6H_5SO_2$ with C_6H_5 to form $(C_6H_5)_2SO_2$ might be unimportant,

$$C_6H_5SO_2 + C_6H_5 \rightarrow (C_6H_5)_2SO_2, \quad \Delta H = -298 \text{ kJ mol}^{-1}, \tag{3}$$

because we did not observe features attributable to $(C_6H_5)_2SO_2$. The reaction of Cl with $C_6H_5SO_2$ to form C_6H_5Cl and SO_2,

$$C_6H_5SO_2 + Cl \rightarrow C_6H_5Cl + SO_2, \quad \Delta H = -204 \text{ kJ mol}^{-1}, \tag{4}$$

is expected to be negligible because it is expected to have a large barrier.

We fit the decay profile of $C_6H_5SO_2$ with a single exponential function and derive a first-order rate coefficient $k_2^I = (3.1 \pm 0.1) \times 10^4$ s^{-1}. The listed errors represent one standard deviation in fitting. An exponential rise with a rate co-

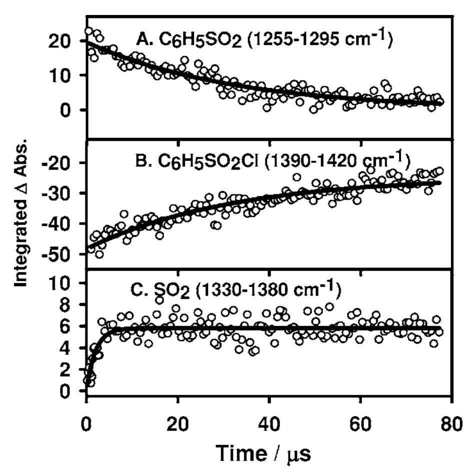

FIG. 8. Temporal profiles of (A) $C_6H_5SO_2$, integrated for 1255–1295 cm^{-1}, (B) $C_6H_5SO_2Cl$, integrated over 1390–1420 cm^{-1}, and (C) SO_2, integrated over 1330–1380 cm^{-1}, all bands were recorded upon photolysis of a flowing mixture of $C_6H_5SO_2Cl/N_2$ (1/240) at 353 K and 72 Torr. The fitted results are represented by solid lines, see text.

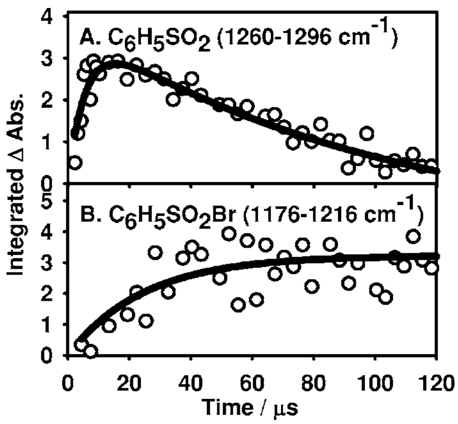

FIG. 9. Temporal profiles of (A) the A1 band of $C_6H_5SO_2$, integrated over 1260–1296 cm^{-1} and (B) the B2 band of $C_6H_5SO_2Br$, integrated over 1176–1216 cm^{-1}, both bands were recorded upon 248 nm photolysis of a flowing mixture of $C_6H_5Br/SO_2/CO_2$ (1/4.4/118) at 30.9 Torr at 298 K. The fitted results are represented by solid lines, see text.

efficient of $k_2^I = 3.1 \times 10^4$ s^{-1} was employed to fit the experimental temporal profile of $C_6H_5SO_2Cl$. The fitting is satisfactory. We are unable to determine the concentration of the Cl atoms, hence precluding determination of an accurate bimolecular rate coefficient k_2. A rough estimate of $[Cl] = (1-5) \times 10^{14}$ molecules cm^{-3} yields $k_2 = (2-10) \times 10^{-11}$ cm^3 molecule^{-1} s^{-1}, consistent with the expectation of a radical-radical reaction.

The production of SO_2 follows first-order kinetics with a rate coefficient $k_5^I = (5.0 \pm 0.6) \times 10^5$ s^{-1}; the listed errors represent one standard deviation in fitting. The rapid time constant derived from the temporal profile of SO_2 is unlikely to be attributed to the three-body dissociation channel [reaction (1c)] because this channel is energetically disfavored. It is likely that SO_2 is generated from the secondary reaction of $ClSO_2$ and C_6H_5,

$$C_6H_5 + ClSO_2 \rightarrow C_6H_5Cl + SO_2, \quad \Delta H = -362 \text{ kJ mol}^{-1}, \tag{5}$$

which is expected to be rapid. The concentration of SO_2 remains nearly constant at the later period. The presence of this rapid reaction is also consistent with the absence of $ClSO_2$ absorption in observed spectra.

2. Irradiation of $C_6H_5Br/SO_2/CO_2$

In the experiment with $C_6H_5Br/SO_2/CO_2$ (1/4.4/118) with a total pressure of ~30.9 Torr, the temporal profile of the SO_2-antisymmetric stretching band of $C_6H_5SO_2$ (integrated over 1260–1296 cm^{-1}) is shown in Fig. 9(A). Fitting the temporal profile of $C_6H_5SO_2$ to a simple model with first-order rise (rate coefficient k_f^I) and decay (rate coefficient k_d^I) yields $k_f^I = (1.2 \pm 0.3) \times 10^5$ s^{-1} and $k_d^I = (2.1 \pm 0.2) \times 10^4$ s^{-1}, respectively. The listed errors represent one standard deviation in fitting.

The rise is associated with the reaction

$$C_6H_5 + SO_2(+M) \rightarrow C_6H_5SO_2(+M), \tag{6}$$

whereas the decay is expected to be associated mainly with the reaction

$$C_6H_5SO_2 + Br(+M) \rightarrow C_6H_5SO_2Br(+M). \tag{7}$$

Assuming that the reaction is in the high-pressure regime and $[SO_2] = 3.5 \times 10^{16}$ molecule cm^{-3}, and considering possible systematic errors, we estimate the bimolecular reaction coefficient $k_6 = (3.4 \pm 1.2) \times 10^{-12}$ cm^3 molecule^{-1} s^{-1}. This rate coefficient of the reaction $C_6H_5 + SO_2$ was unreported. Compared with the bimolecular rate coefficient $(2.9 \pm 0.4) \times 10^{-13}$ cm^3 molecule^{-1} s^{-1} for the reaction of $CH_3 + SO_2$ (Refs. 38 and 39) at 298 K, k_6 is greater by approximately an order. In contrast, k_6 is about one-half of the rate coefficient 8×10^{-12} cm^3 molecule^{-1} s^{-1} for the reactions of C_6H_5 with NO_2 (Ref. 40).

The temporal profile shown in Fig. 9(B) for the SO_2-symmetric stretching band of $C_6H_5SO_2Br$ (integrated over 1176–1216 cm^{-1}) was fitted with a single exponential rise to yield $k^I = (3.0 \pm 0.8) \times 10^4$ s^{-1}. This value is similar to the $k_d^I = (2.1 \pm 0.2) \times 10^4$ s^{-1} derived from the decay of $C_6H_5SO_2$. This result supports that $C_6H_5SO_2Br$ is formed via the secondary reaction of $C_6H_5SO_2$ and Br [reaction (7)].

V. CONCLUSION

We demonstrate an application of time-resolved Fourier-transform absorption technique to detect the SO_2-symmetric and SO_2-antisymmetric stretching bands of the transient species $C_6H_5SO_2$ upon photolysis of gaseous $C_6H_5SO_2Cl$ in N_2 and mixtures of C_6H_5X (X═Cl or Br), and SO_2 in CO_2. Although a fully resolved rotational spectrum is unavailable, our spectrum conforms satisfactorily to a simulation based on rotational parameters derived from quantum-chemical calculations. Observed vibrational wave numbers 1087.7 and 1278.2 cm^{-1} and relative IR intensities are also consistent with those of the SO_2-symmetric and SO_2-antisymmetric stretching modes, respectively, of $C_6H_5SO_2$ predicted with theoretical calculations. Absorption of $C_6H_5SO_2Br$ and $C_6H_5SO_2Cl$ was also observed at the later period after laser irradiation. $C_6H_5SO_2Br$ and $C_6H_5SO_2Cl$ were produced from secondary reactions of $C_6H_5SO_2$ with Br and Cl, respectively. Absorption bands of $C_6H_5SO_2$, SO_2, $C_6H_5SO_2Br$, and $C_6H_5SO_2Cl$ were probed to provide kinetic information. Rate coefficient of the reaction $C_6H_5 + SO_2$ was determined for the first time.

ACKNOWLEDGMENTS

The authors thank the National Science Council of Taiwan (Grant No. NSC95-2119-M-009-032), the MOE-ATU Project of the National Chiao Tung University for support, and V. Stakhursky and T. A. Miller for providing the SPECVIEW software for spectral simulation.

[1] S.-F. Wang, C.-P. Chuang, and W.-H. Lee, Tetrahedron **55**, 6109 (1999).
[2] M. McMillan and W. A. Waters, J. Chem Soc. B **1966**, 422.
[3] A. G. Davies, B. P. Roberts, and B. R. Sanderson, J. Chem. Soc., Perkin Trans. 2 **1973**, 626.
[4] M. Geoffroy and E. A. C. Lucken, J. Chem. Phys. **55**, 2719 (1971).
[5] C. Chatgilialoglu, B. C. Gilbert, and R. O. C. Norman, J. Chem. Soc., Perkin Trans. 2 **1979**, 770.
[6] C. Chatgilialoglu, D. Griller, and M. Guerra, J. Phys. Chem. **91**, 3747 (1987).
[7] H. H. Thoi, O. Ito, M. Iino, and M. Matsuda, J. Phys. Chem. **82**, 314 (1978).

[8] J. E. Bennett, G. Brunton, B. C. Gilbert, and P. E. Whittall, J. Chem. Soc., Perkin Trans. 2 **1988**, 1359.
[9] S.-H. Chen, L.-K. Chu, Y.-J. Chen, I.-C. Chen, and Y.-P. Lee, Chem. Phys. Lett. **333**, 365 (2001).
[10] L.-K. Chu, Y.-P. Lee, and E. Y. Jiang, J. Chem. Phys. **120**, 3179 (2004).
[11] L.-K. Chu and Y.-P. Lee, J. Chem. Phys. **124**, 244301 (2006).
[12] J. Eberhard, P.-S. Yeh, and Y.-P. Lee, J. Chem. Phys. **107**, 6499 (1997).
[13] Y.-J. Chen, L.-K. Chu, S.-R. Lin, and Y.-P. Lee, J. Chem. Phys. **115**, 6513 (2001).
[14] E. Y. Jiang, Spectroscopy (Eugene, Or.) **17**, 22 (2002).
[15] W. Uhmann, A. Becker, C. Taran, and F. Siebert, Appl. Spectrosc. **45**, 390 (1991).
[16] P. Grammaticakis, Bull. Soc. Chim. Fr. **16**, 761 (1949).
[17] M. Rasmusson, R. Lindh, N. Lascoux, A. N. Tarnovsky, M. Kadi, O. Kühn, V. Sundström, and E. Åkesson, Chem. Phys. Lett. **367**, 759 (2003).
[18] M. J. Frisch, G. W. Trucks, H. B. Schlegel *et al.*, GAUSSIAN 03 Revision A.7, Gaussian Inc., Pittsburgh, PA, 2003.
[19] A. D. Becke, J. Chem. Phys. **98**, 5648 (1993).
[20] C. Lee, W. Yang, and R. G. Parr, Phys. Rev. B **37**, 785 (1988).
[21] J. P. Perdew, Phys. Rev. B **33**, 8822 (1986).
[22] T. H. Dunning, Jr., J. Chem. Phys. **90**, 1007 (1989).
[23] D. E. Woon and T. H. Dunning, Jr., J. Chem. Phys. **98**, 1358 (1993).
[24] NIST/EPA Gas-Phase Infrared Database, NIST Standard Reference Database 35, U. S. Department of Commerce, National Institute of Standards and Technology, Gaithersburg, MD, 2004.
[25] L. S. Rothman, C. P. Rinsland, A. Goldman *et al.*, J. Quant. Spectrosc. Radiat. Transf. **60**, 665 (1998).
[26] R. W. Kilb, J. Chem. Phys. **23**, 1736 (1955).
[27] M. H. Sirvetz, J. Chem. Phys. **19**, 938 (1951).
[28] M. Bahou, S.-F. Chen, and Y.-P. Lee, J. Phys. Chem. A **104**, 3613 (2000).
[29] I. I. Kandror, R. G. Gasanov, and R. Kh. Freidlina, Tetrahedron Lett. **14**, 1075 (1976).
[30] T. Ichimura, Y. Mori, H. Shinohara, and N. Nishi, Chem. Phys. **189**, 117 (1994).
[31] H. Zhang, R.-S. Zhu, G.-J. Wang, K.-L. Han, G.-Z. He, and N.-Q. Lou, J. Chem. Phys. **110**, 2922 (1999).
[32] C. Clerbaux and R. Colin, J. Mol. Spectrosc. **165**, 334 (1994).
[33] V. Stakhursky and T. A. Miller, 56th OSU International Symposium on Molecular Spectroscopy, Columbus, Ohio, 2001 (unpublished); SPECVIEW: Simulation and Fitting of Rotational Structure of Electronic and Vibronic Bands, http://www.chemistry.ohio-state.edu/~vstakhur
[34] C. Chatgilialoglu, D. Griller, J. M. Kanabus-Kaminska, and F. P. Lossing, J. Chem. Soc., Perkin Trans. 2 **1994**, 357.
[35] S. W. Benson, Chem. Rev. (Washington, D.C.) **78**, 23 (1978).
[36] W. Tsang, in *Energetics of Organic Free Radicals* edited by J. A. M. Simoes, A. Greenberg, and J. F. Liebman (Academic, London, 1996), p. 22.
[37] M. W. Chase, Jr., J. Phys. Chem. Ref. Data Monogr. **9**, 1 (1998).
[38] F. C. James, J. A. Kerr, and J. P. Simons, J. Chem. Soc., Faraday Trans. 1 **69**, 2124 (1973).
[39] A. J. Frank and F. Turecek, J. Phys. Chem. A **103**, 5348 (1999).
[40] M. Preidel and R. Zellner, Ber. Bunsenges. Phys. Chem. **93**, 1417 (1989).